ACADEMIC PRESS

Journal of Solid State Chemistry 169 (2002) 96–102

JOURNAL OF SOLID STATE CHEMISTRY

www.academicpress.com

Crystal structure predictions: the crystal and electronic structure of $Zr_{1-\delta}V_{1+\delta}As$

Enkhtsetseg Dashjav, Chi-Shen Lee, and Holger Kleinke*

Department of Chemistry, University of Waterloo, Waterloo, Ont., Canada N2L 3G1

Received 30 April 2002; received in revised form 15 July 2002; accepted 27 August 2002

Abstract

$Zr_{1-\delta}V_{1+\delta}As$ is accessible via arc-melting of different mixtures of ZrAs, VAs, Zr, and V. It crystallizes in the tetragonal La_2Sb type, with a phase range of $-0.43(4) \leqslant \delta \leqslant 0.15(1)$. The lattice dimensions ($a = 382.4(1)$ pm, $c = 1486.8(6)$ pm for $Zr_{1.43(4)}V_{0.57}As$; and $a = 375.77(7)$ pm, $c = 1400.2(3)$ pm for $Zr_{0.85(1)}V_{1.15}As$) strongly depend on δ because of the different sizes of the Zr and V atoms. The ZrVAs structure comprises sheets of (empty) M_6 octahedra, whose triangular faces are capped by the main group atoms Q. The sheets are interconnected via $M-Q$ bonds to a truly three-dimensional structure. Like in the isostructural ZrTiAs, the smaller 3*d* M atom prefers the site in the densely packed square planes. In addition to the dominating $M-As$ bonds, the structure comprises strong $M-M$ bonding. Independent of the exact Zr:V ratio, $Zr_{1-\delta}V_{1+\delta}As$ is calculated to have three-dimensional metallic properties.

Keywords: Crystal structure; Electronic structure; Structure map; Arsenides

1. Introduction

Recently, a structure map was developed for metal-rich pnictides and chalcogenides M_2Q, using a structural factor as the ordinate, namely the averaged coordination number of the Q atoms $\langle CN(Q) \rangle$, and a combination of atomic factors as the abscissa, namely principal quantum numbers, valence-electrons, and radii [1]. M stands for all metal atoms of groups 3–5, and Q for the elements of the groups 15 and 16, excluding the elements of the second period, N and O. This includes the ternaries $(M, M')_2Q$ [2] and $M_2(Q, Q')$ (a review about chalcogenides [3]). The today known 34 representatives of this class [4–12] all exhibit Q atoms located in fragments of deltahedral tetrakaidecahedra formed exclusively by M atoms, and infinite M atom substructures of different kinds. The latter may be reminiscent of the various metal structures, i.e., hexagonal or cubic closed packing (*hcp*/*fcc*) as well as cubic body-centered (*bcc*) packing. Although the sulfide Ta_2S [13] stands out in this class, for it is the only structure where the M atoms form chains of centered icosahedra, it still fits into the structure map.

Reasonable separation of the first eleven structure types (Zr_6STe_2 [10] was not uncovered at that point) was achieved by plotting the semi-empirical power product $\mathbf{f} = vec_M \times n_M^2 \times (r_M/r_Q)/(8 - e_Q)^2$ versus the averaged coordination number of the Q atoms $\langle CN(Q) \rangle$. Therein, vec_M represents the valence-electron concentration per M atom after (formally) reducing the Q atoms, n_M the principal quantum number of the M atoms, (r_M/r_Q) the radius ratios based on the Slater radii [14], and $(8-e_Q)$ the electron deficit of the Q atoms in analogy to the (8–N) rule.

Since all of the factors that build **f** are directly accessible, we can calculate **f** for hypothetical, still uncovered M_2Q binaries as well as $M_{2-\delta}M'_\delta Q$ and $M_2Q_{1-\delta}Q'_\delta$ ternaries. Then, the domain and thus the structure type can be predicted. In addition, a transfer of the principles applied for the M_2Q compounds to the M_5Q_3 compounds is possible, and was already used to predict the structures of Ti_5Sb_2Se [15] and Ti_4MoAs_3 [16]. Table 1 provides the **f** values of previously identified M_2Q representatives with $\langle CN(Q) \rangle = 9$, as well as some hypothetical compounds which should fall

*Corresponding author. Fax: 519-746-0435.
E-mail address: kleinke@uwaterloo.ca (H. Kleinke).

0022-4596/02/$ - see front matter © 2002 Elsevier Science (USA). All rights reserved.
PII: S0022-4596(02)00030-0

Table 1
Overview of M_2Q representatives with $\langle CN(Q) \rangle = 9$. Hypothetical compounds are in italic

Compound	Structure type	vec_M	n_M	r_M/pm	r_Q/pm	e_Q	**f**
HfNbP	Co_2Si	3	5.5	150	100	5	15.13
TaVP	Co_2Si	3.5	5	140	100	5	13.61
ZrNbP	Co_2Si	3	5	150	100	5	12.50
HfVAs	Predicted Co_2Si	3	5	145	115	5	10.51
HfTiP	Predicted Co_2Si	3	5	147.5	100	5	10.24
HfTiAs	Predicted Co_2Si	2.5	5	147.5	115	5	8.91
V_2P	Co_2Si	3.5	4	135	100	5	8.40
ZrTiP	Co_2Si	2.5	4.5	147.5	100	5	8.30
ZrVAs	La_2Sb	3	4.5	145	115	5	8.51
La_2Sb	La_2Sb	1.5	6	195	145	5	8.07
Zr_2Sb	La_2Sb	2.5	5	155	145	5	7.42
ZrTiAs	La_2Sb	2.5	4.5	147.5	115	5	7.22
Sc_2Sb	Cu_2Sb	1.5	4	160	145	5	2.94

into that regime. It must be noted that the Co_2Si domain overlaps with the Zr_2P domain; it is evident that ternaries with two distinctly different M atoms (like Zr/Ti, or Hf/Nb) in a ratio close to 1:1 prefer the Co_2Si type, or more precisely, its ordered variant, the TiNiSi type.

Based on Table 1, we foresaw the structure type of ZrTiAs correctly [11]. $Zr_{1-\delta}V_{1+\delta}As$, on the other hand, is at the border of the Co_2Si and La_2Sb domains, depending on the exact Zr:V ratio. In this case, the structure map would predict the formation of the Co_2Si type with $Zr:V \geqslant 1$, and the formation of the La_2Sb type with $Zr:V < 1$. Since structure maps usually are not that precise at the domain borders, the type of $Zr_{1-\delta}V_{1+\delta}As$ cannot be reliably proposed. However, the averaged coordination number of the As atoms should clearly be nine, since this is a common feature of both likely types. As it turned out during our investigations, $Zr_{1-\delta}V_{1+\delta}As$ occurs in the La_2Sb type over the whole phase range of $-0.43(4) \leqslant \delta \leqslant 0.15(1)$, thus with $Zr:V > 1$ as well as $Zr:V < 1$. With this article, we report on its synthesis, structure, and electronic properties.

2. Experimental

2.1. Synthesis

The synthesis of such a metal-rich arsenide (i.e., with an M:As ratio of 2) has to be carried out at elevated temperatures, too high for conventional silica tube techniques. That also prohibits the use of elemental arsenic, for this would either evaporate in an open system, or react with our standard reaction containers like tantalum or molybdenum crucibles. Therefore, we prepared ZrAs as well as VAs in fused silica tubes at 800°C on a scale of several grams, starting from the elements in the stoichiometric 1:1 ratio. All these elements are available from ALDRICH in powder form with purity of 99.5%, and were used as acquired.

The main reactions were then subsequently carried out by arc-melting. This step was prepared by pressing mixtures of ZrAs and VAs with additional elemental zirconium and vanadium in different Zr:V, but fixed (Zr + V):As ratios of 2. These pellets were then arc-melted twice on a water-cooled copper hearth under a flow of Argon. Weight losses were typically of the order of 1–3 wt%. ZrVAs was prepared by arc-melting of a pressed pellet comprising 5/3 mmol VAs and 5/3 mmol Zr. All attempts to synthesize this metal-rich arsenide at temperatures below 1300°C failed.

2.2. Analysis

Based on the powder diagram obtained from the ground sample of the initial composition "ZrVAs", we tentatively assigned the La_2Sb type because of the strong analogy with the powder diagram of ZrTiAs. The reflections were slightly shifted towards larger Bragg angles, which indicates a smaller unit cell, as expected based on the smaller size of a V atom compared to a Ti atom. EDS analyses (LEO 1530, with integrated EDAX Pegasus 1200) on three selected crystals revealed the presence of zirconium, vanadium and arsenic in the anticipated ratio of 33(2):31(2):36(2) [in atomic percent]. Annealing of this sample for a week at 1150°C in a Ta crucible sealed under Argon did not result in disproportionation of ZrVAs. It is therefore concluded that this is indeed the thermodynamically preferred phase at these conditions.

2.3. Phase range

Subsequently, we investigated the phase range of $Zr_{1-\delta}V_{1+\delta}As$, motivated by the observation of mixed Zr/V occupancies in the zirconium vanadium antimonides $(Zr,V)_{13}Sb_{10}$ [17] $(Zr,V)_{11}Sb_8$ [18], and

$Zr_{2+\delta}V_{6-\delta}Sb_9$ [19] as well as a significant phase range in $Zr_{1-\delta}Ti_{1+\delta}As$. We tried to prepare $Zr_{1-\delta}V_{1+\delta}As$ with $\delta = \pm 0.5$, 0, and ± 0.25 by carrying out the following reactions in the arc-melter using the conditions described above:

$$\tfrac{1}{2}\,Zr + ZrAs + \tfrac{1}{2}\,V \rightarrow Zr_{1-\delta}V_{1_{+\delta}}As + Zr_3As + ?, \quad \text{(I)}$$

$$\tfrac{1}{4}\,Zr + ZrAs + \tfrac{3}{4}\,V \rightarrow Zr_{1.25}V_{0.75}As, \quad \text{(II)}$$

$$ZrAs + V \rightarrow ZrVAs, \quad \text{(III)}$$

$$\tfrac{3}{4}\,Zr + \tfrac{1}{4}V + VAs \rightarrow Zr_{1-\delta}V_{1+\delta}As + V_3As + ?. \quad \text{(IV)}$$

The products indicated were identified by X-ray powder diffractograms. No side products were detected in reactions (II) and (III), which strongly suggests the existence of $Zr_{1.25}V_{0.75}As$ and ZrVAs. The slightly different positions of the observed reflections indicate different unit cell dimensions, as expected based on the different sizes of the Zr and V atoms. Using an Inel powder X-ray diffractometer equipped with a position sensitive detector (Cu$K\alpha$1 radiation), we determined the lattice dimensions of $Zr_{1-\delta}V_{1+\delta}As$ of reactions (I) and (IV) based on a body-centered tetragonal cell to be $a = 379.68(9)$ pm and $c = 1484.6(5)$ pm for the Zr-rich case (I) and $a = 375.09(7)$ pm and $c = 13.979(3)$ pm for the V-rich case (IV). Since side products were found in reactions (I) and (IV), it can safely be concluded that the phase range is smaller than $-0.5 \leqslant \delta \leqslant 0.25$.

2.4. Crystal structure determination

In order to determine the phase range more accurately and to prove the formation of the La_2Sb type, we performed single crystal studies on single crystals of reactions (I) and (IV). We mounted prismatic shaped single crystals on the Smart Apex CCD diffractometer using Mo$K\alpha$ radiation. In both cases, 606 frames were collected with 0.3° scans in ω for exposure times of 60 s per frame. The data were corrected for Lorentz and polarization effects. The unit cell dimensions and the systematic absences ($h + k + l = 2n + 1$ for all reflections) were in agreement with the $I4/mmm$ space group of the La_2Sb type as observed for ZrTiAs. This was subsequently confirmed by the successful structure refinements using SHELXL [20] yielding satisfying residual factors (e.g., $R1$ of 0.043 and 0.034, respectively). As expected, the unit cells determined from the single crystals resemble the ones from the powder data, indicating that the crystals selected are indeed typical for the respective samples.

Of the two metal atom sites (which both have the same multiplicity of 4), at least one must be mixed occupied if the stoichiometry differs from ZrVAs. Since the reactions investigated ((I) and (IV)) aimed at the compositions "$Zr_{1.5}V_{0.5}As$" and "$Zr_{0.75}V_{1.25}As$", we initially allowed for mixed occupancies of both metal atom sites, *4e* and *4c*. In ZrTiAs, the *4e* site is exclusively occupied by Zr atoms and *4c* by Ti atoms, which form a dense square planar net. As it turned out, mixed occupancies are present only on one site in both cases analyzed here; in the Zr-rich case (reaction (I)), *4e* is a pure Zr site, and *4c* exhibits a Zr:V ratio of 0.43(4):0.57, resulting in the refined formula $Zr_{1.43(4)}V_{0.57}As$. More or less the reversed is true in the V-rich case (reaction (IV)): *4e* shows some V incorporation (15(1) %), while *4c* is a pure V site. This yields a refined formula of $Zr_{0.85(1)}V_{1.15}As$. Crystallographic details are given in Tables 2 and 3. Further details of the crystal structure investigations can be obtained from the Fachinformationszentrum Karlsruhe, 76344 Eggenstein-Leopoldshafen, Germany, on quoting the depository numbers CSD-412519 and CSD-412520.

Based on the powder diffraction data, it was concluded that the phase range of $Zr_{1-\delta}V_{1+\delta}As$ must be smaller than $-0.5 \leqslant \delta \leqslant 0.25$, but larger than $-0.25 \leqslant \delta \leqslant 0$. This can now be stated more precisely: the range under the experimental conditions used (i.e., synthesis from the melt under exclusion of air) is within $-0.43(4) \leqslant \delta \leqslant 0.15(1)$.

2.5. Electronic structure calculations

We carried out self-consistent tight-binding *first principles* LMTO calculations (LMTO = linear muffin tin orbitals) [21–23] on ZrVAs using the structural parameters obtained from the refinement of $Zr_{0.85}V_{1.15}As$ (i.e., using Zr parameters for $M(1)$ and V parameters for $M(2)$). In the LMTO approach, the density functional theory is used with the local density approximation (LDA). The integration in k space was performed by an improved tetrahedron method [24] on a grid of 641 irreducible k points of the first Brillouin zone. Void space was filled with one so-called empty sphere.

3. Results and discussion

3.1. Crystal structure

The arsenide $Zr_{1-\delta}V_{1+\delta}As$ crystallizes in an ordered variant of the La_2Sb type, the aristotype of which is CeScSi [25]. This structure may be described based on (distorted) M_6 octahedra, whose triangular faces are capped by the main group element Q (left part of Fig. 1), as known from the M_6Q_8 clusters of, e.g., the Chevrel phases. The Q atoms, on the other hand, are surrounded by 9 M atoms that form a tri-capped trigonal prism (deltahedral tetrakaidecahedron, right part of Fig. 1).

These octahedra are interconnected via common corners to form sheets parallel to the *a,b*-plane. Three-dimensionality results from the body-centering symmetry

Table 2
Crystal data and structure refinements

Empirical formula	$Zr_{1.43(4)}V_{0.57}As$	$Zr_{0.85(1)}V_{1.15}As$
Formula weight (g/mol)	234.50	211.14
Temperature (K)	293(2)	293(2)
Wavelength (pm)	71.073	71.073
Space group	*I*4/*mmm*	*I*4/*mmm*
Unit cell dimensions, *a* (pm)	382.4(1)	375.77(7)
c (pm)	1486.8(6)	1400.2(3)
V (nm^3)	0.2174(1)	0.19771(6)
Z	4	4
Calculated density (mg/m^3)	7.16	7.09
Absorption coefficient (mm^{-1})	23.93	26.00
F(000)	413	374
Crystal size (μm)	$30 \times 20 \times 20$	$41 \times 36 \times 27$
Theta range for data collection	5.51–30.01°	2.91–34.99°
Reflections collected	430	1051
Independent reflections (R_{int})	104 (0.0450)	160 (0.0344)
Absorption correction	Sadabs	Sadabs
Max. and min. transmission	1.00 and 0.74	1.00 and 0.58
Data/restraints/parameters	104/0/12	160/0/12
Goodness-of-fit on F^2	1.16	1.10
R indices (all data): $R(F), R_w(F^2)$	0.043, 0.095	0.034, 0.074
Extinction coefficient	0.0020(20)	0.0000(14)
Largest diff. Peak and hole ($e/Å^3$)	1.45 and −1.95	2.75 and −1.37

Table 3
Atomic coordinates and equivalent isotropic displacement parameters ($pm^2 \times 10^{-1}$)

Atom	Site	*x*	*Y*	z^a	z^b	$U_{eq}{}^a$	$U_{eq}{}^b$	occ[a]	occ[b]
M(1)	4*e*	0	0	0.3212(2)	0.3270(1)	17(1)	8(1)	1 Zr	0.85(1) Zr, 0.15 V
M(2)	4*c*	0	1/2	0	0	28(2)	11(1)	0.43(4) Zr, 0.57 V	1 V
As	4*e*	0	0	0.1329(2)	0.1290(1)	17(1)	10(1)		

[a] $Zr_{1.43}V_{0.57}As$.
[b] $Zr_{0.85}V_{1.15}As$.

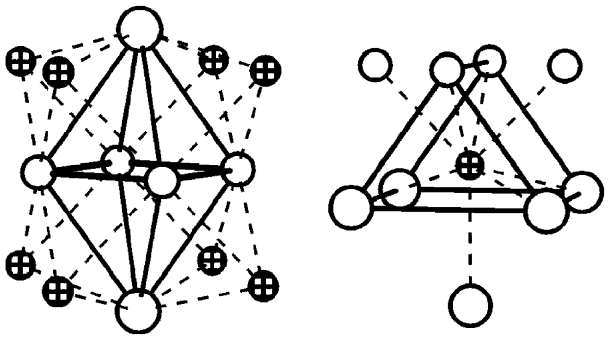

Fig. 1. $Zr_2V_4As_8$ octahedron (left) and Zr_5V_4As tetrakaidecahedron (right). Large, white circles: Zr; small, white: V; medium, hatched: As.

$(x, y, z- > x+\frac{1}{2}, y+\frac{1}{2}, z+\frac{1}{2})$. Thereby, the *M* atoms at the apices of one sheet (*M*(1), *4e* position) are situated directly either above or below the *Q* atoms of the adjacent sheet (Fig. 2). The *M*(1) sites are predominated by the Zr atoms, as in the structure of ZrTiAs. In ZrTiAs as well as in ZrVAs, the 3*d* metal atoms (here: V) prefer the *M*(2) sites that form the square nets (Wyckoff notation *4c*). Since ZrVAs can be prepared both with a Zr:V ratio higher and lower than 1, Zr atoms can partially replace the V atoms and vice versa.

The *M*(1) site, predominated by the Zr atoms, is surrounded by five As atoms at distances between 273 and 280 pm, while the *M*(2) site, dominated by the less electropositive and smaller V atoms, is coordinated by only four As atoms at distances between 261 and 275 pm, depending on the stoichiometry, i.e., the Zr:V ratio (Table 4). The same trends were found in the structure of ZrTiAs. Since the Zr−Sb distances of the two Zr sites of the isostructural Zr_2Sb [26] are almost indistinguishable (298–299 pm), we conclude that the number of surrounding As atoms determine the site preferences, and then the different sizes of Zr and V (e.g., Slater radii: 155 and 135 pm, respectively) lead to differences in the *M*−As bond lengths. With the Slater radius for the As atom being 115 pm, all of the above-mentioned *M*−As bonds are slightly longer than the sum of the radii, indicating strong bonding interactions.

In the structure of ZrVAs and ZrTiAs, the 3*d* metal atom dominated *M*(2) sites form square planar nets that

are twice as densely packed than the $M(1)$ nets. This results in short $M(2)-M(2)$ distances of 266–270 pm for $Zr_{1-\delta}V_{1+\delta}As$ and 268 pm for ZrTiAs, and longer $M(1)-M(1)$ distances of 342–343 pm. The shortness of the $M(2)-M(2)$ distances will also favor an occupation of the $M(2)$ sites by the small $3d$ metal atoms. Intermediate $M-M$ interactions occur between $M(1)$ and $M(2)$, with distances between 307 and 327 pm, whose bonding character will be discussed below.

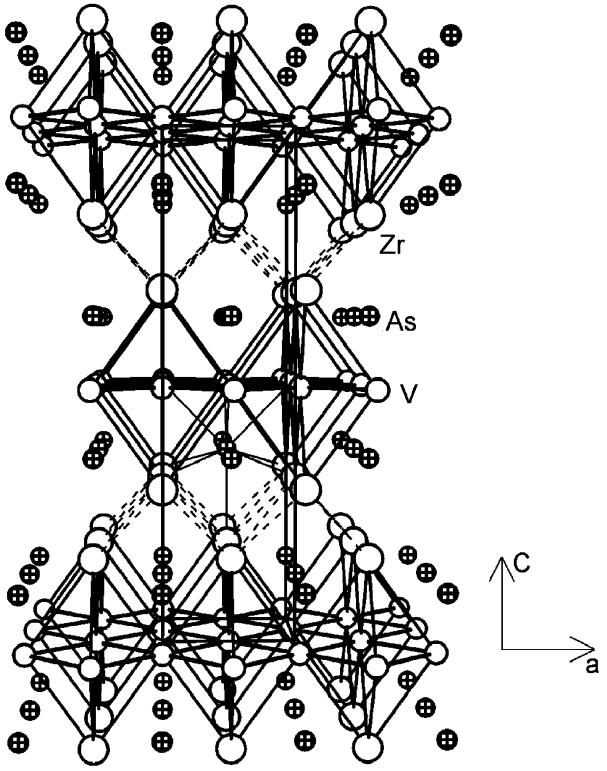

Fig. 2. Crystal structure of ZrVAs in a projection along [010], emphasizing the sheets of M atom octahedra. Large, white circles: Zr; small, white: V; medium, hatched: As.

3.2. Electronic structure

The structure map used to predict the crystal structures of these compounds is based on the assumption that all valence-electrons available for $M-M$ bonding are actually used for this, i.e., no antibonding states are filled. To verify whether this is true in this case, we calculated the electronic structure first, to then subsequently extract this information from the COHP curves (COHP = crystal orbital Hamilton population) [27].

The projection of the band structure onto the densities of states is depicted in the left part of Fig. 3. The 4*s* states of As are located below the energy window shown. The area between −7 and −2 eV is dominated by the As 4*p* states, while the contributions of Zr and V at this energy range indicate covalent Zr−As and V−As bonding, respectively. The peaks between −2 and +2 eV are almost entirely comprised of Zr and V *d* states, with a significant density of states directly at the Fermi level that indicated metallic character, independent of the exact Zr:V ratio.

Five different kinds of significant interactions are present in the structure of ZrVAs. These are both $M-As$ interactions, Zr−As and V−As, and all three kinds of possible $M-M$ bonds, namely Zr−Zr, Zr−V, and V−V. All these are shown in the right and middle part of Fig. 3, respectively.

As in the structure of ZrTiAs, only bonding states are filled, although ZrVAs exhibits a higher valence-electron concentration. However, the number of valence-electrons are close to the border of filling antibonding interactions, a fact that is evident from the $M-M$ COHP curves.

To provide more details on the different interactions, all different integrated COHP values (ICOHPs) are listed in Table 4, together with the respective values of ZrTiAs. ICOHPs may be used to compare relative bond strengths in analogy with the better-known Mulliken overlap populations (MOPs) [28] obtained from extended Hückel approximations. It must be noted in this context that strong bonds are reflected in large positive

Table 4
Selected interatomic distances (pm) and ICOHP values (eV per bond)

		d^a	d^b	ICOHP^b	d^c	ICOHP^c
$M(1)-As$	4*x*	278.9(1)	272.78(6)	−1.53	277.73(5)	−1.57
$M(1)-As$	1*x*	280.0(3)	277.3(2)	−1.31	282.3(1)	−1.35
$M(1)-M(2)$	4*x*	327.4(2)	306.59(9)	−0.99	325.88(9)	−0.77
$M(1)-M(1)$	4*x*	343.4(2)	342.1(1)	−0.30	340.7(1)	−0.40
$M(2)-M(2)$	4*x*	270.40(7)	265.71(5)	−2.08	268.19(4)	−1.97
$M(2)-As$	4*x*	275.0(2)	260.59(9)	−1.79	270.48(8)	−1.58

[a] $Zr_{1.43}V_{0.57}As$.
[b] $Zr_{0.85}V_{1.15}As$; ICOHP values calculated for idealized ZrVAs.
[c] ZrTiAs.

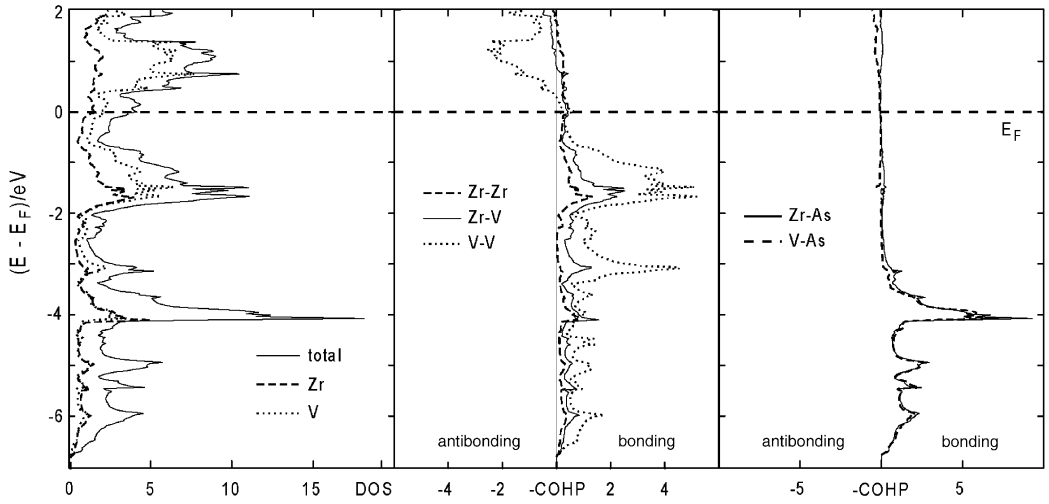

Fig. 3. Electronic structure of ZrVAs. Left: densities of states; middle and right: COHP curves of the different interactions, cumulated for the whole primitive unit cell.

MOPs, but large negative ICOHPs, and that ICOHPs have different units (eV per bond) and higher absolute values. To our knowledge, the first published ICOHPs are −1.53 and −1.00 for the strongest bonds in elemental (*bcc*) iron and nickel, respectively [29]. A more recent article [30] compares Zr−Zr and Sb−Sb ICOHPs of different interactions of selected compounds as well as elements. For example, the strong Zr−Zr bonds in the hexagonal close packed element have ICOHPs of −1.30 and −1.25 eV per bond for the bonds of 318 and 323 pm.

These are significantly stronger and shorter than the Zr−Zr bonds in ZrVAs (−0.30, 342 pm) and ZrTiAs (−0.40, 341 pm). For comparison, we calculated the ICOHPs of elemental vanadium (cubic body-centered packing) as well. The shortest V−V bond in elemental vanadium of 262 pm comprises an ICOHP of −1.89 eV per bond, which is almost identical in length and strength with the strong V−V bond in ZrVAs (−2.08 eV per bond, 266 pm). The Zr−V bonds exhibit intermediate ICOHPs with −0.99, but are hard to compare due to the lack of a well-defined standard. Overall it is noted, that all $M-M$ bonds listed in Table 4 are significantly bonding, yet differ in strength.

4. Summary

The structure map for M_2Q compounds published in the year 2000 predicted a coordination number of nine for the As atoms of $Zr_{1-\delta}V_{1+\delta}As$. Since ZrVAs is situated right at the domain border between two structure types, namely La_2Sb and Co_2Si, a precise prediction of its structure was virtually impossible. However, the coordination number was foreseen correctly, and the structure type turned out to be one of the two likely candidates, La_2Sb. Increasing the tendency towards $M-M$ bonding by either adding more valence-electrons or replacing the 4*d* by 5*d* *M* atoms (e.g., substitute Zr with Hf) or the 3*d* by 4*d* *M* atoms (e.g., substitute V with Nb) is predicted to lead to the formation of the Co_2Si type.

$Zr_{1-\delta}V_{1+\delta}As$ is a metallic conductor, independent of the Zr:V ratio, as our *first principles* electronic structure calculations revealed. The structure of ZrVAs is mainly stabilized by strong Zr−As, V−As, and V−V bonding, and additionally by intermediate Zr−V and weaker Zr−Zr bonds. No significant As−As contacts are present, which is typical for such a metal-rich arsenide.

Acknowledgments

Financial support from NSERC, CFI, OIT, the Province of Ontario (Premier's Research Excellence Award for H.K.) and the Canada Research Chair program is appreciated.

References

[1] H. Kleinke, B. Harbrecht, Z. Anorg. Allg. Chem. 626 (2000) 1851.
[2] L. Zeng, H.F. Franzen, J. Alloys Compd. 270 (1998) 119 (ZrHfP).
[3] B. Harbrecht, T. Degen, M. Conrad, J. Alloys Compd. 246 (1997) 37.
[4] The older examples may be found in: P. Villars, Pearson's Handbook, Desk Edition, American Society for Metals, Materials Park, OH, 1997.
[5] P.A. Maggard, J.D. Corbett, Angew. Chem. Int. Ed. 36 (1997) 1974 (Sc_2Te).
[6] T.E. Weirich, S. Hovmöller, A. Simon, 16th Nordic Structural Chemistry Meeting, Sigtuna, Sweden, 1998, p. 44 (β-Ti_2Se).
[7] G. Örlygsson, B. Harbrecht, Inorg. Chem. 38 (1999) 3377 (Zr_2Te).

[8] B. Harbrecht, M. Conrad, T. Degen, R. Herbertz, J. Alloys Compd. 255 (1997) 178 (Hf_2Te).
[9] H. Kleinke, D. Evans, B. Harbrecht, Z. Kristallogr. Suppl. 16 (1999) 43 (Zr_4SbSe).
[10] G. Örlygsson, M. Conrad, B. Harbrecht, Z. Anorg. Allg. Chem. 627 (2001) 1017 (Zr_6STe_2).
[11] C.-S. Lee, E. Dashjav, H. Kleinke, Chem. Mater. 13 (2001) 4053 (ZrTiAs).
[12] G.A. Marking, H.F. Franzen, J. Alloys Compd. 204 (1994) L16 (ZrNbP and HfNbP).
[13] H.F. Franzen, J.G. Smeggil, Acta Crystallogr. 25B (1969) 1736.
[14] J.C. Slater, J. Phys. Chem. 41 (1964) 3199.
[15] H. Kleinke, J. Alloys Compd. 336 (2002) 132.
[16] C.-S. Lee, E. Dashjav, H. Kleinke, J. Alloys Compd. 338 (2002) 60.
[17] H. Kleinke, Chem. Commun. (Cambridge) (1998) 2219.
[18] H. Kleinke, J. Mater. Chem. 9 (1999) 2703.
[19] H. Kleinke, Eur. J. Inorg. Chem. (1998) 1369.
[20] G.M. Sheldrick, SHELXTL-V5.1, University of Göttingen, Germany, 1998.
[21] L. Hedin, B.I. Lundqvist, J. Phys. C 4 (1971) 2064.
[22] O.K. Andersen, Phys. Rev. B 12 (1975) 3060.
[23] H.L. Skriver, The LMTO Method, Springer, Berlin, 1984.
[24] P.E. Blöchl, O. Jepsen, O.K. Andersen, Phys. Rev. B 49 (1994) 16223.
[25] I.R. Mokra, O.I. Bodak, Dopov. Akad. Nauk Ukr. RSR A 4 (1979) 312.
[26] E. Garcia, J.D. Corbett, J. Solid State Chem. 73 (1988) 440.
[27] R. Dronskowski, P. Blöchl, J. Phys. Chem. 97 (1993) 8617; see also http://www.cohp.de.
[28] R.S. Mulliken, J. Chem. Phys. 23 (1955) 2343.
[29] G.A. Landrum, R. Dronskowski, Angew. Chem. Int. Ed. 39 (2000) 1560.
[30] I. Elder, C.-S. Lee, H. Kleinke, Inorg. Chem. 41 (2002) 538.